minerals

MDPI

Article

Analysis of Controlling Factors of Pore Structure in Different Lithofacies Types of Continental Shale—Taking the Daqingzi Area in the Southern Songliao Basin as an Example

Xinrui Wang [1], Yu Sun [1,2,*], Tianxu Wang [3], Baiquan Yan [1,2] and Ruhao Liu [4]

[1] School of Earth Science, Northeast Petroleum University, Daqing 163318, China; wangxr_2017@163.com (X.W.)
[2] Sanya Offshore Oil & Gas Research Institute, Northeast Petroleum University, Sanya 572024, China
[3] Exploration and Development Research Institute of Jilin Oilfield, Songyuan 138000, China
[4] Institute of Unconventional Oil and Gas Development, Chongqing University of Science and Technology, Chongqing 401331, China
* Correspondence: sunyu_hc@163.com

Abstract: Due to the influence of terrigenous debris, the internal pore structure of continental shale is highly heterogeneous, and the controlling factors are complex. This paper studies the structure and controlling factors of shale reservoirs in the first member of the Qingshankou Formation in the Southern Songliao Basin using core data and various analytical test data. The results show that the original deposition and subsequent diagenesis comprehensively determine the shale reservoirs' pore structure characteristics and evolution law. According to the severity of terrigenous debris, the shale reservoirs in the study area are divided into four categories and six subcategories of lithofacies. By comparing the characteristics of different shale lithofacies reservoirs, the results show that the lithofacies with a high brittle mineral content have more substantial anti-compaction effects, more primary pores to promote retention and a relatively high proportion of mesopores/macropores. Controlling the organic matter content when forming high-quality reservoirs leads to two possibilities. An excessive organic matter content will fill pores and reduce the pore pressure resistance. A moderate organic matter content will make the inorganic diagenesis and organic hydrocarbon generation processes interact, and the development of organic matter mainly affects the development of dissolution pores. The comprehensive results show that A3 (silty laminated felsic shale) reservoirs underwent the pore evolution process of "two drops and two rises" of compaction, cementation and pore reduction, dissolution and pore increase, and organic matter cracking and pore increase, and they are the most favourable lithofacies of the shale reservoirs in the study area.

Keywords: Songliao Basin; lithofacies type; pore structure; pore evolution

Citation: Wang, X.; Sun, Y.; Wang, T.; Yan, B.; Liu, R. Analysis of Controlling Factors of Pore Structure in Different Lithofacies Types of Continental Shale—Taking the Daqingzi Area in the Southern Songliao Basin as an Example. *Minerals* **2024**, *14*, 1025. https://doi.org/10.3390/min14101025

Academic Editor: Luca Aldega

Received: 16 August 2024
Revised: 20 September 2024
Accepted: 11 October 2024
Published: 13 October 2024

1. Introduction

The United States has experienced a technological revolution in shale oil over the past two decades, achieving the economically viable scale development of hydrocarbon resources in shales such as the Bakken Formation in the Williston Basin and the Eagle Ford Formation in the Western Gulf Basin, thereby transforming the global energy market [1,2]. Distinct from North American marine shales, China's shale oil resources are predominantly terrestrial, characterised by complex tectonics, a low level of maturity, well-developed laminations, frequent sedimentary facies changes, and a pronounced heterogeneity in both macro-distribution and micropore structures [3]. Since shale oil is primarily contained within nanoscale pores [4–6], the pore structure features, including the volume, type and size of storage spaces, significantly impact the oil-bearing capacity and occurrence of shale oil reservoirs [5–7]. Consequently, reservoir pore structure serves as a crucial factor in assessing the quality of fine-grained sedimentary reservoirs, directly determining

their storage capacity and exploration potential [8–10]. Thus, studying pore structure characteristics and evolution patterns has remained a focal point in shale reservoir research.

Experimental equipment often limits the characterisation of pore structures. The characterisation techniques of shale microscopic pore structure can be roughly divided into two categories: qualitative description and quantitative characterisation. Among them, experimental methods such as optical microscopy, field emission scanning electron microscopy, focused ion beam scanning electron microscopy (FIB-SEM) and micro- and nano-CT scanning can be used to intuitively and finely observe the pore structure morphology [8,10,11]. However, limited by a high resolution, these instruments can only describe the local pore structure pattern, and the obtained pore information is highly homogeneous and not very representative. The gas (CO_2 or N_2) adsorption method [12,13], constant-speed/high-pressure mercury injection [14,15], nuclear magnetic resonance [16] and gas pulse permeability tests can characterise a wide range of pore areas, and the characteristics of reservoir spaces are easy to quantify. However, each method has unique characteristics, and several methods need to be combined to achieve comprehensive pore-size characterisations [17–19]. Effectively integrating different results, systematically analysing the characteristics of shale reservoir spaces and comprehensively characterising pore types and structural characteristics are key to the quantitative characterisation of reservoir pore characteristics.

The formation and evolution of shale reservoirs are mainly affected by organic–inorganic factors [6,7,20]—for example, organic matter cracking pores [21,22], clay transformation [23,24], and quartz and carbonate cementation [25,26]. However, the current research on reservoir controlling factors pays more attention to one aspect: the study of pore evolution during diagenesis. For example, organic matter produces organic acids, which can dissolve minerals [27,28]. The production of hydrocarbons will cause overpressure and inhibit the reduction in porosity to a certain extent [6,7,29]. It generally involves clay mineral transformation, siliceous cement formation, feldspar dissolution, organic matter evolution and the reservoir's physical properties. In particular, significant progress has been made in the influence of pore evolution characteristics [30–33]. In addition, in the over-mature stage, the cracking of organic matter will produce organic matter pores [21,34]. However, whether an excessive organic matter content will damage the shale reservoir structure or felsic minerals is still uncertain [35–37]. It has a dual effect on shale. Increasing these mineral contents will increase the compressive strength of shale rocks and provide soluble mineral carriers [38]. However, when their content is too high, they will reduce the abundance of organic matter in continental shale [39]. Clay content has good plasticity and is closely related to organic matter content. Organic matter cracking promotes the transformation of clay [34,40].

However, the above results apply more to the pore structure of high-TOC (Total organic content) black lacustrine shale reservoirs in deep lakes. However, most lacustrine shales are often subjected to terrigenous debris and intravaginal biological and chemical processes and contain interlayers of siltstone/fine sandstone and carbonate rocks [33,34,40,41]. The diversity of the original sedimentary types will significantly influence the original pore structure. Therefore, it is urgent to supplement the research on the difference in the diagenetic evolution path and genetic mechanism of reservoirs with different original sedimentary types and fabrics.

This paper analyses the mature lacustrine shale in the first member of the Qingshankou Formation (Qing1) of the Upper Cretaceous in Changling Sag, Southern Songliao Basin. The essential characteristics of lithofacies and organic matter in the study area are analysed through core and laboratory analyses, and the lithofacies types are divided. The primary characteristics and reservoir space types of the study area's first member of the Qingshankou Formation are determined based on scanning electron microscopy, high-pressure mercury injection, nitrogen adsorption and other analytical testing methods. Based on the fractal theory, the classification standard of fine-grained sedimentary pores in the Qingyi member of the study area is established, and the full-aperture characterisation is realized.

The controlling factors affecting the pore structure of the reservoir are analysed from the perspective of sedimentation and organic matter, and the favourable lithofacies types and pore structure evolution mode of the shale reservoir are determined, which provides a theoretical basis for the selection of this kind of shale oil dessert area.

2. Geological Setting

The Songliao Basin is a large-scale Mesozoic-Cenozoic continental petroleum-bearing sedimentary basin with a dual structural feature of an initial fault depression followed by a superimposed depression in the NNE direction in Northeastern China [42–44]. The basin's foundation consists of Carboniferous-Permian metamorphic rocks and granite. The sedimentary cover includes Jurassic, Cretaceous, Paleogene, Neogene and Quaternary deposits (Figure 1c). Based on the properties of the basement rocks and the regional geological characteristics of the caprock, the depression structural layers in the Songliao Basin can be divided into six first-order structural units, which are believed to control the distribution of reservoirs for oil, natural gas, shale gas and oil sands (Figure 1a,c). Among them, the Central Depression has long been the sedimentary and subsidence centre of the Songliao Basin, with almost all of its strata being well developed. The thickness of the Cretaceous stratum here exceeds 6500 m, containing two sets of high-quality hydrocarbon source rocks: the first member of the Qingshankou Formation and the second member of the Nenjiang Formation [6].

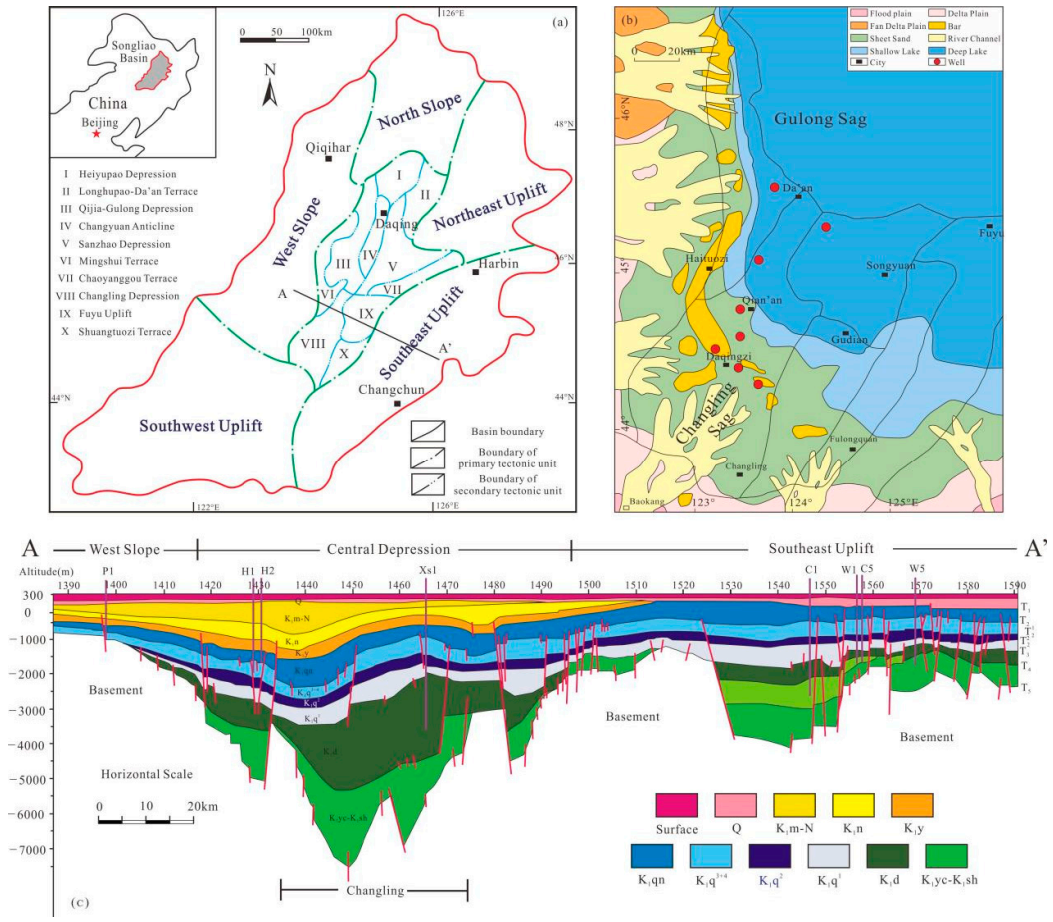

Figure 1. Tectonic position and comprehensive stratigraphic map of the target area in the southern part of the Songliao Basin [45,46]. (**a**) Location map of the Sanzhao depression and tectonic units of the Songliao Basin. The black line (AA') shows the location of the stratigraphic profile (Figure 1c) of the Songliao Basin. (**b**) Sedimentary facies distribution of Changling Sag in Songliao Basin. (**c**) The stratigraphic section across the central part of the Songliao Basin shows the basin structure.

In the Southern Songliao Basin, the sedimentary system's subsidence rate in the lake basin extension was more significant than the sedimentation rate, leading to the expansion of the lake basin and the formation of lake invasions, with only the Tongyu-Baokang sedimentary system remaining relatively intact. Its depositional end is the Southern Songliao Basin shale area [33,34]. Unlike the shale oil-rich Qijia-Gulong Sag in the north of the Songliao Basin, where dark mudstone and shale rich in organic matter are deposited in deep and semi-deep lake facies, the organic-rich shale in the south is located outside the delta front (shallow lake facies) of the Daqingzi area, which is more severely affected by terrigenous debris (Figure 1b).

The Upper Cretaceous is the primary strata in the middle and shallow layers of the Southern Songliao Basin. It is divided into the Quantou Formation (K_1q), Qingshankou Formation (K_2qn), Yaojia Formation (K_2y), Nenjiang Formation (K_2n), Sifangtai Formation (K_2s) and Mingshui Formation (K_2m) from bottom to top (Figure 2a). Among them, the first member of the Qingshankou Formation is the main stratum for shale oil exploration and development in the Songliao Basin [33,45]. The central depression of the Songliao Basin is separated by the Songhua River, which can be divided into Gulong Sag and Changling Sag. In the lower part of the first member of the Qingshankou Formation in Changling Sag, Southern Songliao Basin, large-scale lake floods have occurred, and lithologic assemblages of organic-rich shale, siltstone and carbonate interbeds have been deposited. The upper part of the first member of the Qingshankou Formation is dominated by organic-rich shale (Figure 2b).

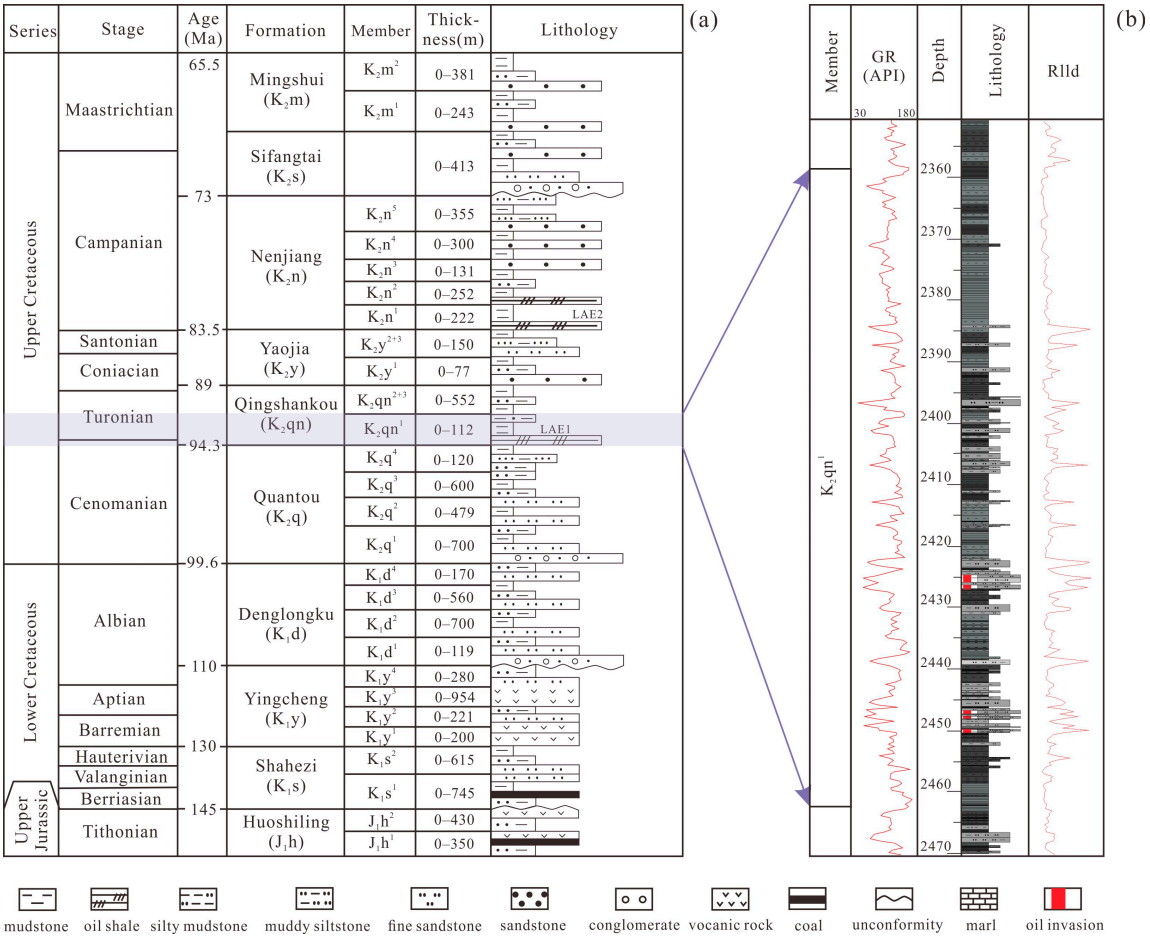

Figure 2. The extent of the target layer and the present study: (**a**) Comprehensive characteristics of the diagenetic system in the basin [45,46]. (**b**) The lithology and logging curve characteristics of typical wells in the study area.

3. Data and Methods

3.1. Samples

The 74 core samples in this study are from 8 critical exploration wells in the first member of the Qingshankou Formation in the Southern Songliao Basin (whose buried depth varies greatly). Figure 1b describes the geographical location of the coring well. Among them, 57 samples (including 45 shale samples) were subjected to TOC tests, X-ray diffraction, vitrinite reflectance, thin-section observation, argon ion polishing field emission scanning electron microscopy, nitrogen adsorption, high-pressure mercury injection, nuclear magnetic resonance and other analytical tests. The maturity of each well is medium (Ro is 1.0%–1.2%). The remaining 17 sandstone samples were analysed for a long time. Only this part of the data is used for the classification of lithofacies types, and this paper does not include the study of pore structure.

3.2. Sample Processing Flow

For the TOC content test, the sample was crushed and pretreated by acidification, washing and drying, and then the TOC content was analysed by a CS-230 carbon-sulphur analyser. The sample was crushed to 200 mesh and prepared on glass slides during XRD whole-rock analysis. An X-ray diffractometer (Model: D8 DISCOVER, UK) was used to test the samples, and the contents of quartz, feldspar, calcite, pyrite and clay minerals were quantitatively identified using the Rietveld full-spectrum simulation method [47].

LTNA and 1-D NMR (Model: D8 GeoSpec2, UK) experiments were used to characterise the shale reservoirs' PSD [48,49]. After washing the sample with oil, grinding it to 60–80 mesh [50] and drying it to remove volatile impurities, an appropriate amount of crushed sample (masses of 1.0 and 2.5 g for shale samples and 4 g for carbonate rock samples) was selected, and the nitrogen adsorption and desorption curves were measured using an specific surface area and porosimetry instrument (Model: ASAP2460-2HD, USA) in the subcritical state (77 K). The specific surface area and PSD were calculated using the Brunauer–Emmett–Teller (BET) and non-local density functional theory (NLDFT) models based on the adsorption curve, respectively. Still, the results can only reflect pores smaller than 200 nm [12,51].

One-dimensional NMR reflects pore size by detecting the relaxation time of the hydrogen nuclei contained in the pores, and the characterised range can vary from a few nanometres to several hundred micrometres. This study used n-dodecane as the saturating medium to prevent clay expansion. The NMR T2 spectra of the samples were measured under dried conditions. The T2 spectrum reflecting the fluid distribution was obtained via basement removal, and the saturated fluid mass and effective porosity were determined using the mass–amplitude conversion relationship.

4. Results

4.1. Shale Lithofacies Types

4.1.1. Basic Petrological Characterisation

Through the meticulous core observation of eight boreholes drilling into the K_2qn^1 Formation in the Daqingzi region, coupled with laboratory thin-section analyses, the lithology of the K_2qn^1 strata in this area was primarily classified into two types: mudstone–shale and siltstone. Based on scanning electron microscopy (SEM) observations and whole-rock mineral X-ray diffraction (XRD) analyses, the mineralogy of the K_2qn^1 mudstone shale is composed primarily of quartz, plagioclase, K-feldspar and clay minerals. Minor amounts of ankerite, calcite, pyrite and siderite are also present. Among the clay minerals, illite is the most predominate, followed by illite/smectite mixed layers, with traces of chlorite (Figure 3a). Examining the ternary diagram of felsic [35–37], clayey and carbonate minerals, it becomes evident that the K_2qn^1 mudstone–shale primarily develops felsic and clayey mudstone–shale, with a minor contribution from dolomitic limestones (Figure 3b). This mineralogical composition reflects the unique sedimentary processes and geochemical environment that shaped the K_2qn^1 Formation in the Daqingzi area.

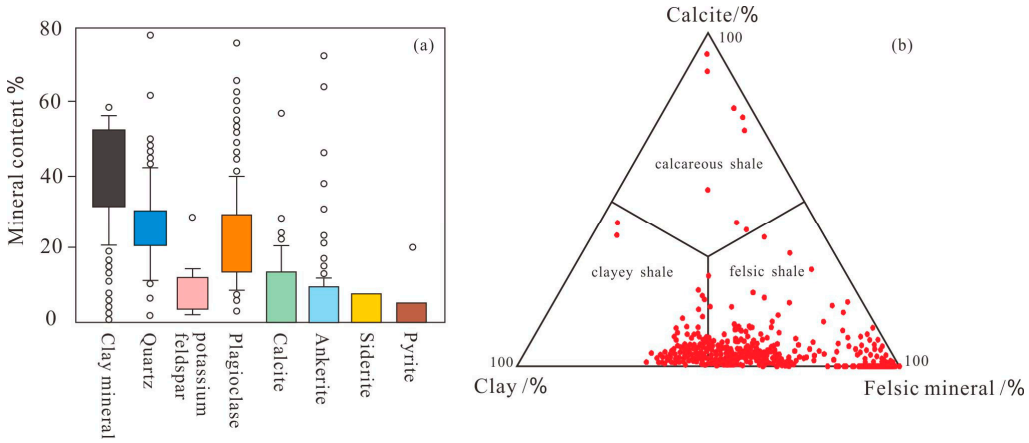

Figure 3. Fundamental petrographic characteristic parameters of the K_2qn^1 reservoir in the Daqingzijing area: (**a**) Box plot of mineral composition, (**b**) triangular diagram of lithological classification.

4.1.2. Sedimentary Structural Characteristics

The fine-grained clastic sediments in the study area are predominantly characterised by laminated, lamellar and massive structures [33]. Transitional lithologies such as siltstone, muddy siltstone and silty mudstone mostly exhibit an enormous structure, accompanied by a considerable amount of deformation and disturbance features. Massive mudstone occurs less frequently within the mudstone shale, and lamination and stratification are more prevalent. Based on grain size, laminae can be further subdivided into silt-grade laminae and mud-grade laminae. Silt-grade laminae possess coarser overall grain sizes, with silt particles (diameter > 4 μm) accounting for over 50% of the content. In contrast, mud-grade laminae display finer grain sizes, with less than 50% of the content consisting of coarser particles (diameter > 4 μm) (Figure 4f,h).

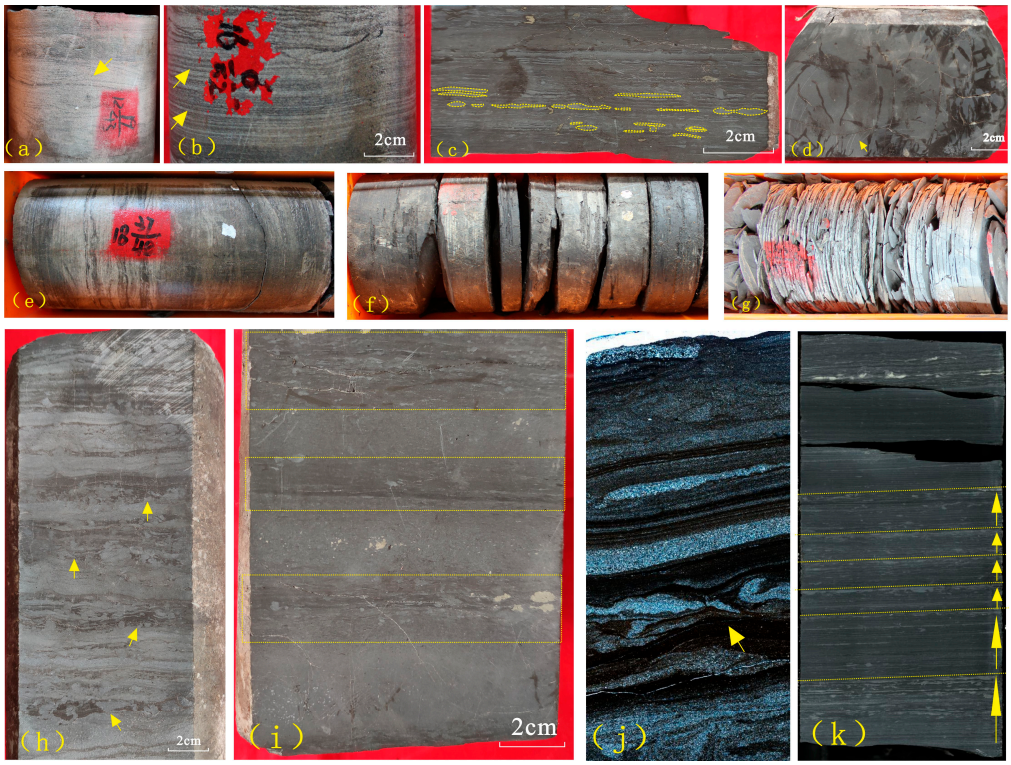

Figure 4. The development characteristics of the sedimentary structure in the first member of Daqingzi. (**a**) Grey white siltstone; wavy bedding; 2129.39 m. (**b**) Gray silty shale; silt lamina and

argillaceous lamina interbedded to form parallel bedding; 2380.02 m. (**c**) Black/grey massive shale; fine silty lamina discontinuous and local silty lenticle; 2101.5 m. (**d**) Black/gray massive mudstone; the main sedimentary structure was destroyed by biological disturbance; 2106.7 m. (**e**–**g**) macroscopic massive, layered and laminated shale. When the content of silty laminae is high and the interbeds are more frequent, it is easier to rupture and form macroscopic laminae structure; 2402.6 m, 2395.43 m, 2379.41 m. (**h**) Gray argillaceous siltston; sand veins, sandy mass, deformation, with obvious characteristics of traction flow structure and showing signs of burrowing; 2151.7 m. (**i**) Black/gray massive mudstone; grain sequence bedding formed by fine silty lenticles and agglomerates in the middle; 2104.4 m. (**j**) silty shale; 2231.70 m. (**k**) Blocky shale; clay lamina felsic lamina interbedded; 2056.39 m.

Laminae with a single layer thickness of $\leq$1 cm are classified as laminated (bedding planes or shales), characterised by variations in colour, grain size and mineral composition between layers (Figure 4b,c,e,f,k). These primarily correspond to shales dominated by different grain-size laminae, suggesting that shales may also contain relatively high silt contents. When the thickness of a single lamina exceeds 1 cm, it is referred to as stratified (Figure 4h,j) and is typically found in transitional lithologies such as silty mudstone and muddy siltstone, where internal deformation structures are common. Laminae thicker than 1 m are massive, lacking distinct internal structures and exhibiting a uniform colour, grain size and mineral composition (Figure 4a,d,i). These are predominantly present in mudstone and siltstone, with locally observed graded bedding and cross-bedding.

4.1.3. Classification of Lithofacies Types

In the previous lithofacies classification scheme, if there are too many indicators, it may lead to confusion on lithofacies types, which is difficult to predict by logging and seismic activity and not easy to popularize; alternatively, if there are too few indicators, it may result in a lack of obvious distinctions between different petrographic phases in terms of their reservoirs and oil-bearing characteristics. Many scholars often use "TOC + structural type + mineral fraction" to classify shale lithofacies types [37–41].

The K_2qn^1 Formation in the study area exhibits many lithofacies types characterised by frequent variations, pronounced lamination and strong heterogeneity. To effectively describe the unique features of these diverse lithofacies, a ternary classification system based on "Sedimentary Structures—Mineral Composition—Lithology" has been employed [33]. Within this framework, the study area primarily encompasses four significant categories, encompassing a total of six lithofacies (Table 1): clay-laminated claystone (A1), clay-laminated felsic shale (A2), silt-laminated felsic shale (A3), massive mudstone (B), silty mudstone and muddy siltstone (C) and siltstone (D) (Figure 5a–f).

Table 1. Lithofacies classification bases of the K_2qn^1 Formation.

Sample Number	Depth (m)	Lithofacies Types	Quartz	Feldspar	Clay Minerals	Mineral Characteristics	Sedimentary Structure Characteristics
A	A1	Clay laminated clayey shale	17.4–33.2 22.55	9.5–18.5 15.47	34.1–46.3 39.12	felsic laminae < clayey laminae	Laminated Single lamina thickness < 1 cm Interbedding of felsic laminae and clayey laminae
	A2	Clay laminated felsic shale	21.7–33.4 28.25	12.9–23.5 18.62	28.4–40.4 36.01	felsic laminae > clayey laminae	
	A3	Silty laminated felsic shale	27.6–35.6 31.78	18.5–26.4 25.3	8.4–39.4 28.29	felsic laminae > 50%	
B	B	Blocky mudstone	25.4–34.1 31.4	15.25–25.7 21.24	20.24–36.1 28.91	Clayey content > 50% Silt-sized particles < 25%	Massive
C	C	Silty mudstone and argillaceous sandstone	31.4–41.1 35.21	24.5–42.7 36.85	10.27–15.1 12.57	Felsic content > 50%	Layered or massive With internal deformation structures present in some parts
D	D	Siltstone	34.7–42.4 38.25	33.2–64.5 51.2	8.4–12.1 11.4	Felsic content > 50% Silt-sized particles > 75%	Layered or massive

Note: 17.4–33.2, 22.55 stands for min. to max. and ave.

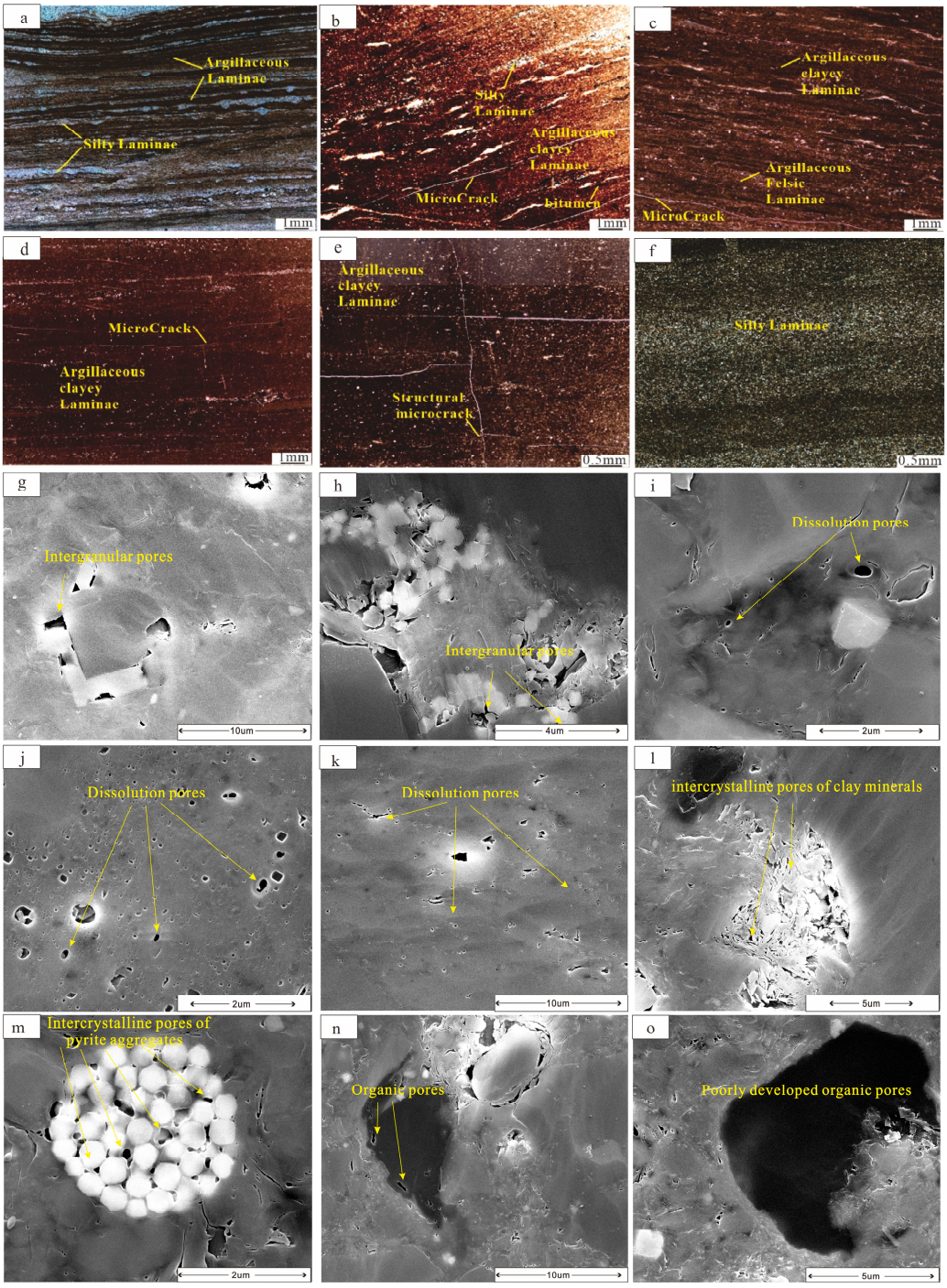

Figure 5. Thin-section characteristics of main shale lithologies in the Qing1 member of the Changling Sag. (**a**) Low-organic-matter-content laminated A3; (**b**) medium-organic-matter-content lamellar A2; (**c**) high-organic-matter-content lamellar A1; (**d**) high-organic-matter-content interlayer microfracture A2; (**e**) high-organic-matter-content interlayer microfracture A2; (**f**) inorganic matter A3; (**g**) interparticle pores in lithofacies type C; (**h**) interparticle pores in lithofacies type A2; (**i**) dissolution pores in lithofacies type A2; (**j**) dissolution pores in lithofacies type A3; (**k**) dissolution pores in lithofacies type A1; (**l**) intercrystalline pores in lithofacies type A1; (**m**) intercrystalline pores within pyrite aggregates in lithofacies type A1; (**n**) organic matter pores in lithofacies type A1; (**o**) poorly developed organic matter pores in lithofacies type A3.

4.2. Differences in the Pore Structures of Different Lithofacies Reservoirs

4.2.1. Differences in Pore Types of Different Types of Lithofacies

The fine-grained sedimentary reservoir within the first section of the Qingshankou Formation exhibits diverse pore types. Drawing upon a comprehensive suite of experiments, including numerous cast thin sections, argon ion polished scanning electron microscopy (SEM), large field-of-view stitched SEM and energy-dispersive X-ray spectroscopy (EDS), this study identified four dominant pore types in the reservoir: interparticle pores, dissolution pores, intercrystalline pores and organic pores. Notably, organic pores are relatively underdeveloped (Figure 5).

The interparticle pores in the study area predominantly exist in the form of micropores or fractures, primarily comprising pore spaces formed by the mutual support between different particles, including brittle particles (quartz, feldspar, carbonate rocks and pyrite) and flexible particles (organic matter and clay minerals). The abundance of interparticle pores is highly susceptible to mechanical compaction and cementation processes. Microscopic observations reveal that these pores often exhibit a polygonal shape, characterised by straight edges and relatively large pore diameters ranging from 200 nm to 1 μm. These pores are developed across various lithofacies types (Figure 5g,h).

The dissolution pores are primarily distributed along the edges of mineral grains, exhibiting a harbour-like or serrated morphology. The pore diameters of interparticle dissolution pores mainly range from 200 nm to 1 μm. These dissolution pores generally exhibit good connectivity, significantly enhancing the reservoir properties of the formation. Intragranular dissolution pores, on the other hand, are primarily developed within feldspar grains, displaying an irregular serrated pattern, with pore diameters distributed mainly from 50 nm to 500 nm (Figure 5i–k).

Intercrystalline pores are predominantly developed between mineral crystals such as pyrite and clay. In the first section of the Qingshankou Formation within the study area, clay mineral-related intercrystalline pores are predominantly present, with pore diameters typically ranging from 100 nm to 500 nm. A minor occurrence of pyrite-related intercrystalline pores is also observed, with pore diameters commonly distributed between 200 nm and 500 nm (Figure 5i,m).

Organic matter pores positively contribute to the adsorptive properties of shale. During the hydrocarbon generation process, organic carbon consumption leads to the formation of organic matter pores within the reservoir. In the first section of the Qingshankou Formation, organic matter pores exhibit complex morphologies within or at the organic matter's edges. The pore diameters typically range from 50 nm to 1 μm, although organic matter pores constitute a relatively small proportion overall (Figure 5n,o).

Among the pore types in various lithofacies of the first section of the Qingshankou Formation in this region, dissolution pores and interparticle pores account for relatively high proportions, averaging approximately 37.1% and 36.9%, respectively. In lithofacies type A3, due to their higher content of brittle minerals, interparticle pores comprise a higher percentage, approximately 39.4%. In lithofacies types C and D, interparticle pores constitute approximately 44.7% of the pore types, while dissolution pores comprise about 33.95%. Intercrystalline pores exhibit similar proportions across all lithofacies, averaging approximately 19.6%. There exist notable differences in the proportion of pore types among various lithofacies, particularly among the mudstone and shale lithofacies types (A1, A2 and A3). Among these, the proportion of intercrystalline pores varies relatively little across lithofacies, whereas interparticle pores, dissolution pores and organic matter pores exhibit regular variations with changes in lithofacies types. As the lithofacies transition from A1 to A3, the content of brittle minerals gradually increases, the TOC content decreases, the clay mineral content rises and the proportion of interparticle pores gradually increases, while the proportions of dissolution pores and organic matter pores gradually decrease (Table 2).

Table 2. Distribution of pore types across diverse lithofacies types.

Lithofacies (Quantity)	Pore (wt.%)	Intercrystalline Pore Percentage (%)	Dissolved Pore Percentage (%)	Intergranular Pore Percentage (%)	Organic Pore Percentage (%)
A1	2.7–4.05 3.21	14.2–22.1 18.6	28.2–48.1 37.3	22.7–31.2 27.1	8.4–12.2 10.1
A2	3.35–5.21 4.21	13.7–23.7 18.1	36.4–51.2 44.2	30.1–39.2 35.2	8.2–10.4 9.4
A3	4.02–6.21 5.27	19.2–24.2 21.1	25.4–43.2 33.1	32.7–49.2 39.4	4.2–8.1 6.4

Note: 2.7–4.05, 3.21 stands for min. to max. and ave.

4.2.2. Differences in Pore Sizes of Different Types of Lithofacies

This study utilizes the self-similarity principle of fractal theory to classify fine-grained sedimentary reservoirs [16,17]. Pores of the same type exhibit identical physical characteristics, known as self-similarity. Based on variations in pore features, pores within sandstone and mudstone reservoirs of fine-grained sediments are systematically categorized. Pores with similar characteristics demonstrate comparable trends, and the inflexion points on the curves align with the pore throat threshold values that signify transitions between pore types. Consequently, the self-similarity evident in the curves, coupled with the relationship diagram between the cumulative porosity and throat radius of key well samples from diverse lithofacies types (Figure 6), reveals that the samples all display four distinct fractal segments. The consistent trends among pores with identical features indicate that the pore systems in the mudstone and shale reservoirs of the study area can be segmented into four types according to the proposed classification scheme. Specifically, the values of lgr = −2.3, lgr = −1.3 and lgr = −0.3 represent the pore throat thresholds for different pore types. Therefore, leveraging the self-similarity observed in the curves, we categorize pores into four classes: macropores (>500 nm), medium pores (50 nm to 500 nm), small pores (5 nm to 50 nm) and micropores (<5 nm).

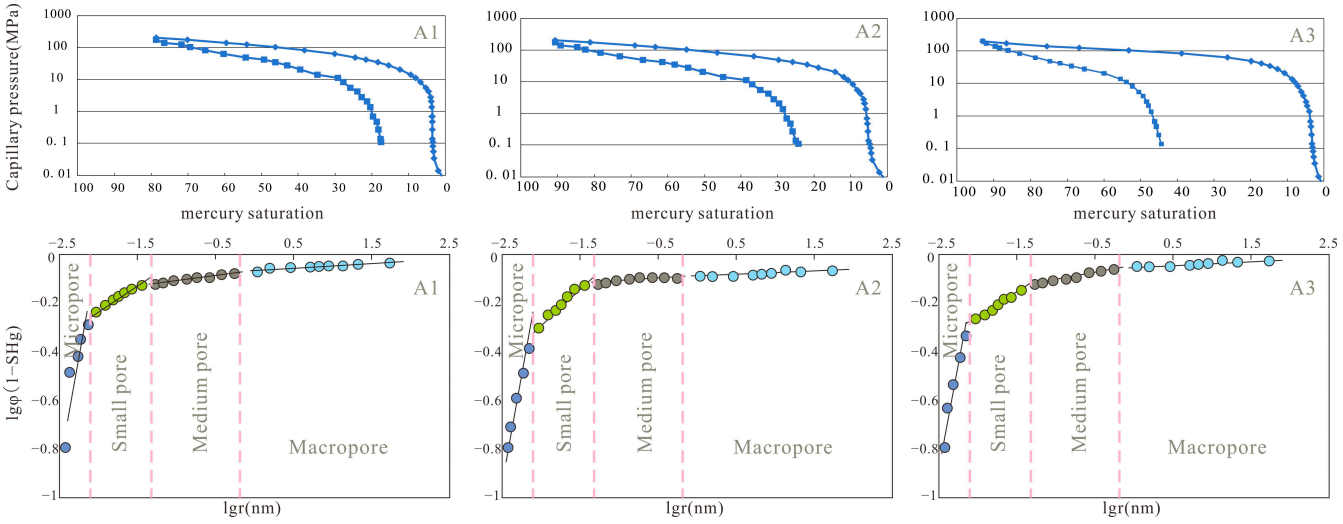

Figure 6. Fractal characteristics of pore throats in fine-grained sediments from the first section of Qingshankou Formation, categorized into four types: macropores (>500 nm), mesopores (50 nm to 500 nm), micropores (5 nm to 50 nm) and nanopores (<5 nm). A1: Clay laminated clayey shale, A2: Clay laminated felsic shale, A3: Silty laminated felsic shale.

Given that the data obtained from the high-pressure mercury injection primarily reflect the pore throat distribution, which deviates from the direct pore distribution, the mercury injection pressures do not often exceed 200 MPa, resulting in the suboptimal characterisation

of micro- and nanopores compared to low-temperature nitrogen adsorption (LTNA). On the other hand, nuclear magnetic resonance (NMR) indirectly characterises pore space by detecting hydrogen nuclei within the rock's storage voids, necessitating a calibration factor to convert hydrogen signals into pore radii. This study employs LTNA to calibrate NMR, enabling comprehensive shale pore size characterisation. Firstly, the pore sizes from LTNA are converted into a cumulative curve. Subsequently, the porosity component values corresponding to each T2 point in NMR are divided by the total porosity to obtain the respective pore proportions. These proportions are then obtained from the most minor to the largest, yielding the NMR pore proportion cumulative curve H(T2). Based on the linear relationship between the NMR relaxation time T2 and pore radius r, H(T2) is transformed into a function of the pore radius H(r/k), where k is the linear coefficient. By iteratively adjusting k, the error between H(r/k) and the cumulative curve G(r) from LTNA is minimized, and the corresponding k value is designated as the calibration factor C. Using r = T2 x C, the NMR T2 spectrum is converted into an NMR pore throat distribution curve, quantitatively depicting the distribution of pore sizes across different ranges and generating a comprehensive pore size distribution map for the samples (Figure 7).

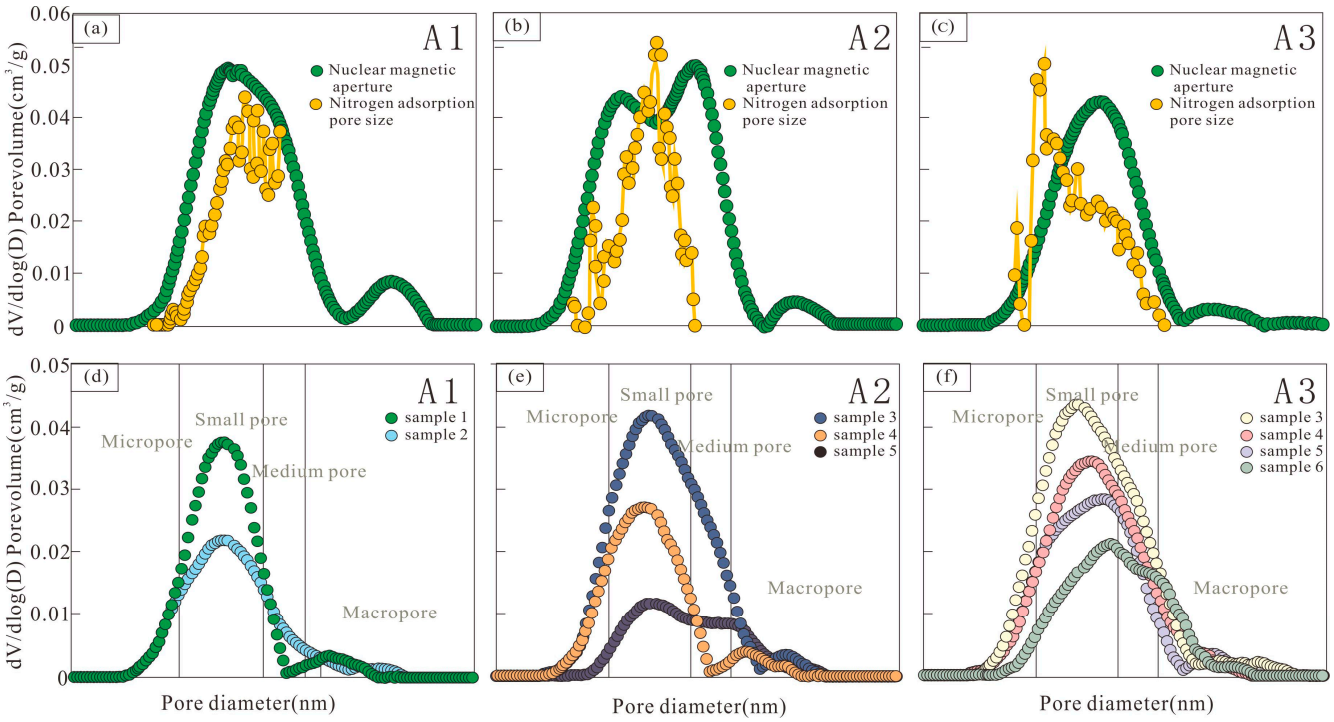

Figure 7. Comparison of pore size distribution between shale from the first section of Qingshankou Formation in the Daqingzijing area. (**a**–**c**) Low-temperature nitrogen adsorption calibration nuclear magnetic resonance diagram. (**d**–**f**) Comparison of pore size distribution of full pore size range. A1: Clay laminated clayey shale, A2: Clay laminated felsic shale, A3: Silty laminated felsic shale.

The calibrated pore size distribution of fine-grained sediments from the first section of the Qingshankou Formation primarily spans 5–1000 nm, with a dominant peak frequently located within 5–100 nm. This indicates a prevalence of medium pores, small pores and micropores in this region's fine-grained sediments. Specifically, mudstones and shales exhibit pore sizes mainly distributed between 1 and 100 nm, while siltstones' pore sizes range predominantly from 10 to 1000 nm, with a dominant peak in the 100–1000 nm range.

The difference in pore size between different lithofacies types is more obvious than that of pore type. Combined with the results of the full pore size characterisation (Table 3), it can be seen that in the four shale lithofacies, all kinds of lithofacies are dominated by micropores and small pores. Among them, the proportion of micropores and small

pores of the A1 type is about 81.1%, the proportion of micropores and small pores of the A2 type is about 76.6%, the proportion of micropores and small pores of the A3 type is about 68.8% and the proportion of micropores and small pores of the B type is about 82.3%. Regarding mesopores and macropores, type A3 lithofacies have a high proportion of mesopores/macropores, with an average proportion of about 31.2%. The proportion of mesopores/macropores in type A1 lithofacies is the lowest, with an average proportion of about 18.9%. It shows that the classification of lithofacies types can effectively characterise the heterogeneity of reservoir characteristics of terrigenous clastic deposits.

Table 3. TOC and pore structure characteristics of lithofacies.

Lithofacies (Quantity)	TOC (wt.%)	Micropore Percentage (%)	Small Pore Percentage (%)	Medium Pore Percentage (%)	Macropore Percentage (%)
A1	0.45–5.7 2.14	35.2–42.2 40.3	28.2–48.1 40.8	10.5–18.4 14.9	1.4–7.4 4.0
A2	0.42–5.1 1.74	26.2–38.4 34.5	36.4–53.2 44.1	10.2–21.5 17.0	1.6–8.4 4.4
A3	0.35–2.9 1.41	17.4–41.2 24.9	37.4–52.1 43.9	24.2–38.7 21.1	7.2–15.1 10.1

Note: 0.45–5.7, 2.14 stands for min. to max. and ave.

5. Discussion

5.1. Influence of Mineral Fraction and Organic Matter on Pore Space

5.1.1. The Influence of Sedimentary Characteristics on Reservoir Pore Structure

The influence of the original deposition on reservoir pores is mainly reflected in mineral composition. The mineral content also has a certain impact on the reservoir characteristics [6,21,25,38]. Because the B type lithofacies are less developed in this area, this paper does not feature a targeted discussion of the controlling factors. This paper analyses the correlation between the pore size distribution characteristics of the three shale lithofacies types mainly developed in the study area and their different mineral contents (Figure 8).

In terms of feldspar content, with the increase in feldspar content, the proportion of micropores decreases, and the proportion of macropores + mesopores increases. In contrast, in A3 type lithofacies, the positive correlation between the feldspar content and the proportion of macropores + mesopores is stronger. This phenomenon is mainly due to the increase in feldspar content, the increase in the direct intergranular pores of brittle minerals and the fact that a part of the intergranular pores can be retained during diagenesis. At the same time, feldspar minerals are dissolved, which further increases the proportion of dissolved pores, resulting in the promotion of the feldspar mineral content to larger pores.

In terms of quartz mineral content, quartz mineral content has a good positive correlation with the proportion of mesopores and macropores in class A lithofacies, a weak positive correlation with the proportion of small pores and a poor correlation with the proportion of micropores. This phenomenon is mainly because in class A mudstone lithofacies, quartz and feldspar belong to brittle minerals with a similar content. Both of them jointly determine the development ratio of larger pores, while the quartz content is not the main controlling factor in small pores and micropores.

An excessive clay content will reduce the reservoir's compaction resistance. On the other hand, clay minerals contain a large number of intercrystalline pores, which leads to an increase in the proportion of micropores. Overall, the clay mineral content of each type of lithofacies is negatively correlated with the proportion of mesopores and macropores and positively correlated with the proportion of micropores and micropores.

Based on the above factors, it can be judged that for the type A lithofacies, quartz and feldspar have an improved effect on mesopores/macropores, and clay minerals will

increase the proportion of micropores and small pores. Therefore, the pore throat structure of the type A3 lithofacies with a higher quartz feldspar content is better.

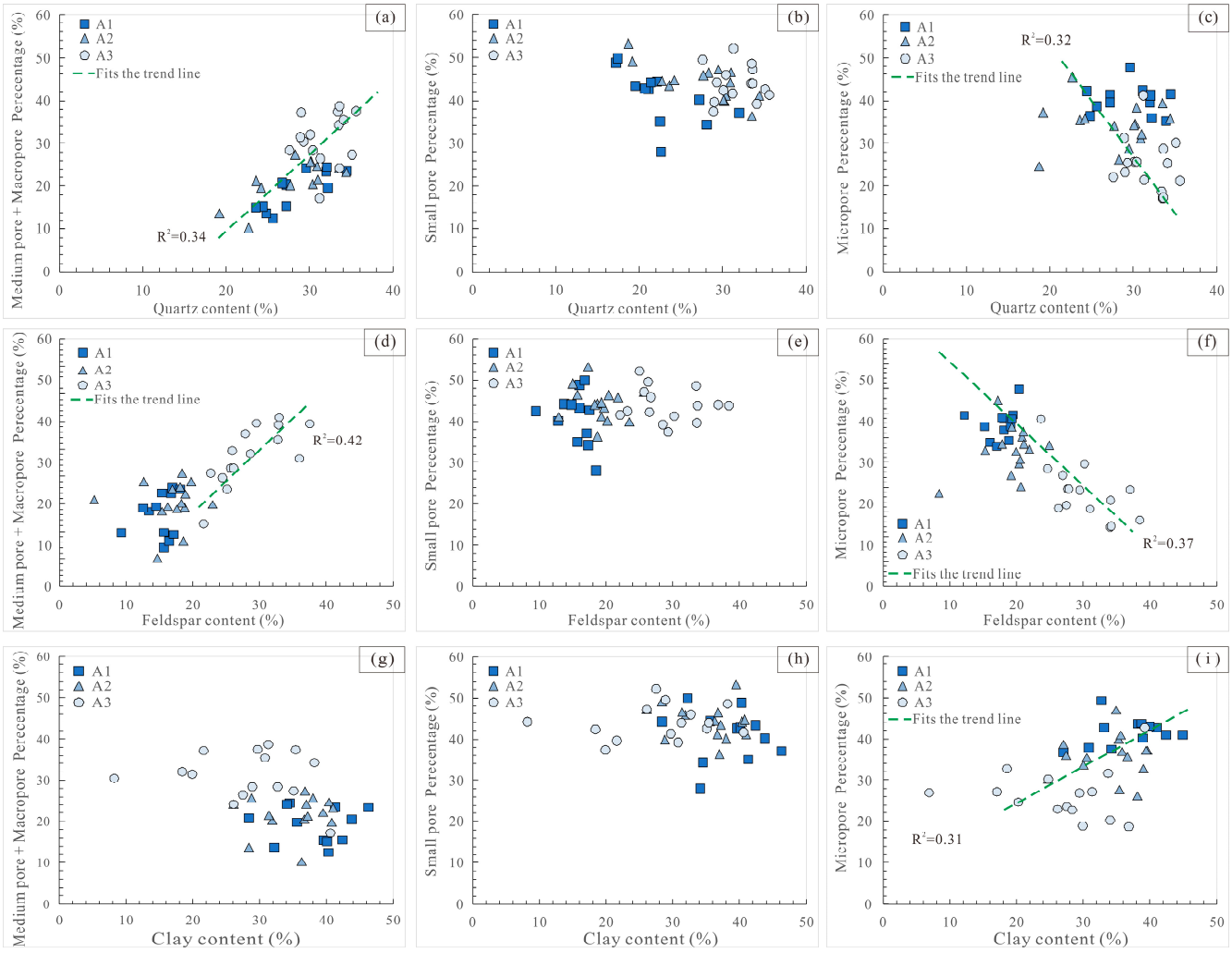

Figure 8. Analysis of the influence of different mineral content on pore structure. (**a**–**c**) The relationship between feldspar content and the proportion of macropores, micropores and micropores in different lithofacies; (**d**–**f**) The relationship between quartz content and the proportion of macropores, micropores and micropores in different lithofacies; (**g**–i) The relationship between clay content and the proportion of macropores, micropores and micropores in different lithofacies.

5.1.2. The Controlling Effect of Organic Matter Characteristics on Reservoir Pore Structure

The content of organic matter in fine-grained sediments also exerts a significant degree of control over the pore structure of reservoirs. By integrating the analysis of organic matter characteristics in the study area, we examine the factors that govern the pore structure characteristics of fine-grained sedimentary reservoirs based on the organic matter content. Tmax is a rapid indicator of organic matter maturity, although its actual results can be influenced by mineral composition and kerogen types. In the first section of the Qingshankou Formation within the study area, the average hydrogen index of fine-grained sediments ranges from 280.6 to 340.9 mg/g. According to the classification standard for organic matter types in source rocks (SY/T5735-2019) [6], the first section of the Qingshankou Formation predominantly comprises Type II kerogen (Figure 9a). Notably, the organic matter in the study area exhibits strong heterogeneity, with a wide distribution span across various lithofacies types (Figure 9b).

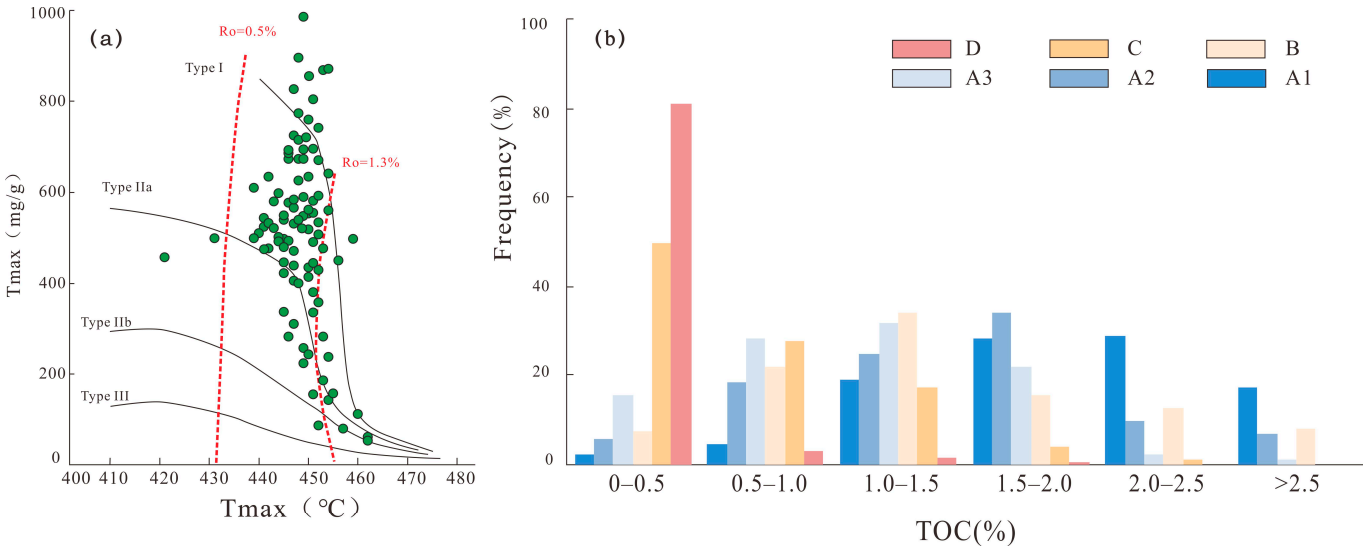

Figure 9. Organic matter characteristics of the first section of Qingshankou Formation. (**a**) Classification of organic matter types in the shale reservoirs of the first section of the Qingshankou Formation was determined based on the relationship between the hydrogen index (HI) and Tmax. (**b**) A statistical analysis is presented of the TOC content distribution characteristics across various lithofacies types within the first section of the Qingshankou Formation in the Daqingzijing area.

The statistical results indicate that the relationship between the total organic carbon (TOC) content and porosity does not always follow a linear pattern [33] (Figure 10a). Instead, an overall trend emerges, initially showing an increase, followed by a deceleration in the rate of increase, and finally, a gradual decline. When the TOC content is small, organic matter plays a positive role in enhancing pore space. Specifically, among various pore size characteristics, the proportion of medium pores and macropores gradually increases with rising TOC content. This is attributed to the fact that within this TOC content range, during hydrocarbon generation, organic acids dissolve minerals such as feldspar, resulting in an overall improvement to the reservoir. The amount of organic matter content is positively correlated with the proportion of dissolution pores (Figure 10d). Additionally, due to the relatively high feldspar content in A3 lithofacies, the increase in medium and macropores is steeper, whereas the rise in A1 and A2 lithofacies is more gradual at this stage.

When the TOC content is high, because the soluble organic matter fills the intergranular pores and the organic matter has flexible characteristics, an excessive organic matter content will reduce the compressive strength of the rock, which is not conducive to pore development. Regarding porosity, with the increase in organic matter content, the porosity and the proportion of mesopores and macropores increase slowly, and even the porosity decreases (Figure 10a,b). In terms of the proportion of micropores, all kinds of lithofacies types increase the proportion of micropores (Figure 10c). That is to say, with the increase in TOC content, some of the macropores and mesopores are filled with organic matter or transformed into micropores or small pores under compaction. At this stage, organic matter plays a destructive role in pore structure. There is a stable positive correlation between the development of organic matter pores and the content of TOC, and the difference between each lithofacies type is small, indicating that the content of organic matter has a significant controlling effect on its pore production (Figure 10e).

In the lithofacies types of categories C and D, the internal organic matter content is extremely low. However, due to the severe interbedding of terrigenous clastic fine-grained sedimentary sandstone and mudstone in this region, the acidic fluids generated by the thermal evolution of organic matter remain to act as significant erosive agents that contribute to pore formation through dissolution under burial conditions. This process leads to an increase in the content of feldspar dissolution pores within the mudstone and adjacent sandstone sections. The graphical representation indicates that as the distance between

the sandstone and adjacent mudstone sections increases, the content of medium pores tends to increase. Additionally, a higher TOC content accelerates the dissolution of brittle minerals within the mudstone and subsequent erosion towards adjacent sandstone sections, resulting in a more significant increase in the proportion of medium pores (Figure 10f).

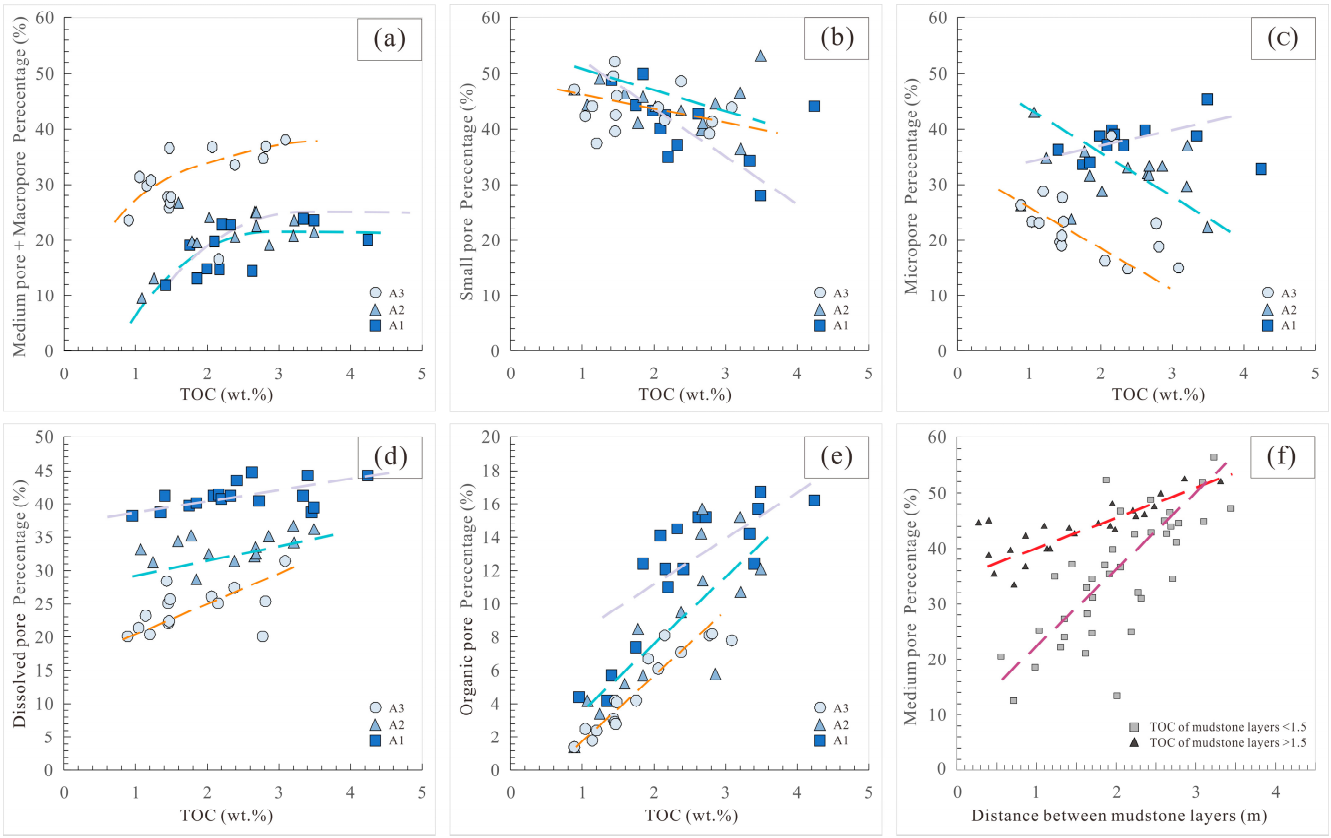

Figure 10. The controlling effect of organic matter content on reservoir characteristics. (**a**–**c**) The correlation between organic matter content and the proportion of mesopores + macropores, micropores and micropores. (**d**) The correlation between organic matter content and the proportion of dissolution pores. (**e**) The correlation between organic matter content and the proportion of organic matter pores. (**f**) The correlation between the proportion of mesopores in sandstone and the distance from mudstone with different TOC content.

5.2. Impact of Diagenesis on Pore Characteristics

5.2.1. Types of Diageneses

The content of quartz and feldspar in the shale reservoir of the first section of the Qingshankou Formation in the study area is high (Table 1). The soluble components provided by these brittle minerals can improve the pores of the shale reservoir [27,28,51–53]. Dissolution is one of the most important pore-increasing effects in the study area. Its occurrence is related to acidic fluids. Before entering the mature stage of organic matter, kerogen cracking produces a large amount of CO_2 and carboxylic acids, which are dissolved with soluble components to form secondary dissolution pores (Figure 11a–c). However, the intensity of dissolution is mainly controlled by two factors, which can be divided into the number of organic acids and the development of fluid exchange pathways. Both determine the pore-increasing efficiency of dissolution. Combined with the energy spectrum and SEM, the influence of feldspar on dissolution is analysed. Taking type A3 lithofacies as an example (Figure 11d), the thin sections show strong dissolution differences. The porosity of the upper part can reach 13%, and the lower part is only 1.5%. From the plane distribution map of elements (Figure 11e–i), the content of each element is similar, indicating that the distribution of inorganic minerals such as feldspar, quartz and calcite

is similar. However, the difference between the upper and lower parts of the C content is obvious, which indicates that the upper part has a higher organic matter content, which can confirm that the TOC content analysed above plays an important role in the occurrence of dissolution [54,55].

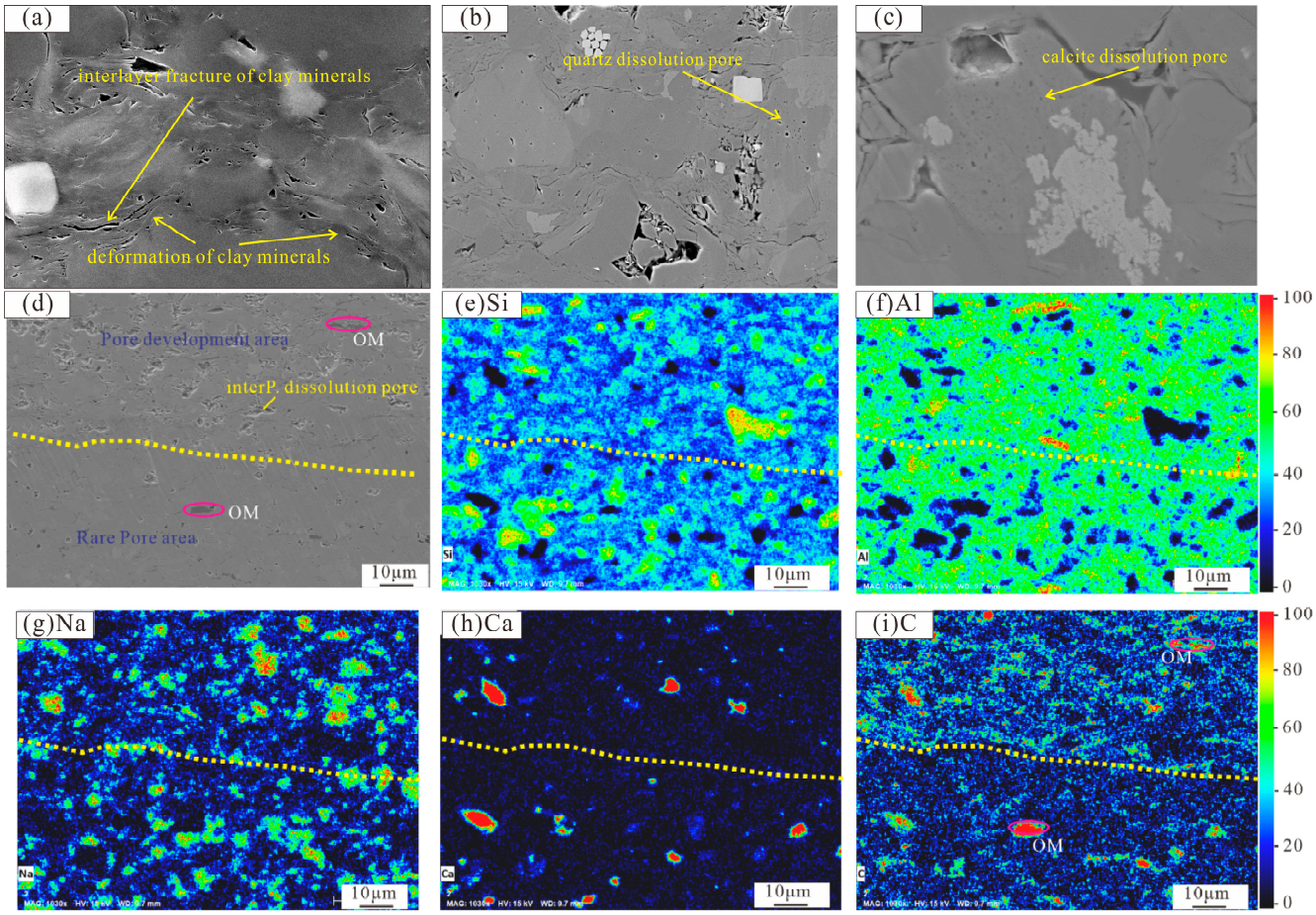

Figure 11. The SEM image and element image of type A3 lithofacies in the study area. (**a**–**c**) Dissolution phenomenon. (**d**) Yellow dotted line represents the boundary between the upper and lower parts, which show different pore development characteristics. (**e**–**i**) represent the spectral distribution of Si, Al, Na, C and C elements, respectively. Except for element C, the difference between the upper and lower elements is relatively small, and the upper part of element C is more developed than the lower part.

5.2.2. Changes in Pore Characteristics during Diagenetic Evolution

Based on the variation patterns of various parameters, the pore evolution can be delineated into four distinct stages (Figure 12). When the Ro maturity value is less than 0.85, compaction dominates diagenesis, leading to a rapid decrease in porosity. During this stage, the proportion of macropores and medium pores decreases while the proportion of small pores increases gradually. The predominant pore types at this stage are intergranular pores and intercrystalline pores.

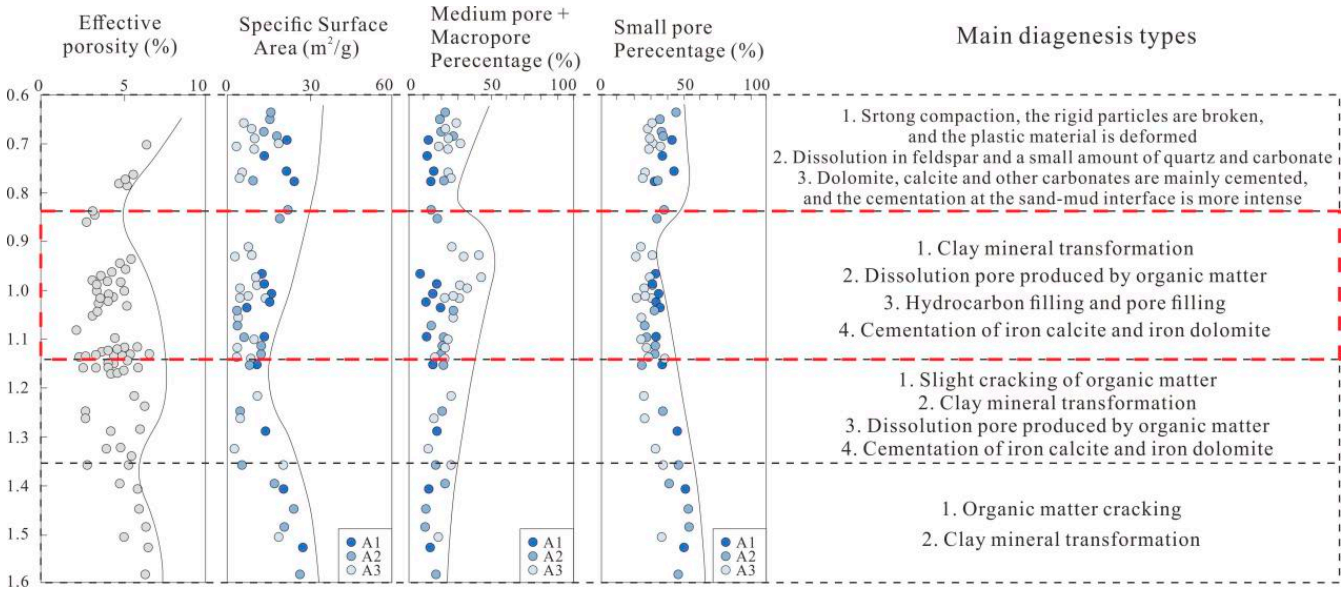

Figure 12. Evolution of shale pore structure in the first section of Qingshankou Formation in the Daqingzijing area.

As Ro ranges between 0.85 and 1.15, dissolution and hydrocarbon generation processes dominate. Affected by dissolution, the porosity exhibits an increasing trend. The proportion of medium pores and macropores increases while the specific surface area decreases, primarily due to the filling of micropores by soluble organic matter. The dominant pore types during this stage are intergranular pores and dissolution pores, with a minor presence of organic pores.

Between Ro values of 1.15 and 1.35, the stages are marked by ferroan dolomite cementation, the enhanced cracking of soluble organic matter and clay transformation. As a result, the porosity and the proportion of macropores and medium pores decrease while the specific surface area increases. This indicates that soluble organic matter or bitumen begins to crack, releasing micropores and small pores. The primary pore types at this stage are intercrystalline pores and a limited number of organic pores.

When Ro exceeds 1.35, the cracking of organic matter and clay transformation intensify further, resulting in the formation of abundant organic pores. Overall, porosity increases while the specific surface area and the proportion of small pores decrease. The proportion of macropores and medium pores continues to decline. The dominant pore types in this final stage are organic pores and intercrystalline pores of clay minerals.

5.2.3. Pore Evolution Model for Dominant Lithofacies Reservoirs

Based on the previous research results, it can be found that among different lithofacies types, A3 lithofacies have a higher porosity and a higher proportion of mesopores/macropores and are often identified as dominant lithofacies reservoirs in the process of production and development. These pore structure characteristics are affected by factors such as mineral content and organic matter content on one hand and organic matter maturity, mechanical compaction and dissolution in the diagenetic process on the other hand. Organic matter is often deposited with clay minerals to form an organic matter–clay mineral complex.

Drawing on the delineation of diagenetic evolution stages and alterations in pore types, a pore evolution model for the premium reservoirs of A3 and D lithofacies is established (Figure 13). At the initial burial stage, when the organic matter maturity is low (Ro < 0.5%), the sedimentary structure is relatively loose. Early compaction leads to a tighter packing of rock grains, resulting in reduced pore sizes and porosity. The dominant pore types are intergranular and intercrystalline pores.

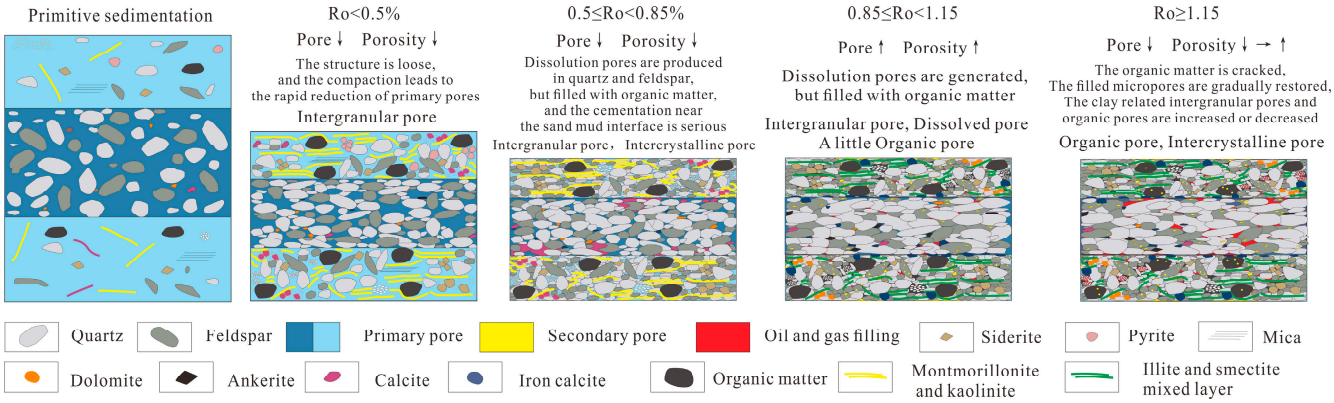

Figure 13. Pore evolution model of shale in the first section of Qingshankou Formation in the Daqingzijing area.

As the burial depth increases, the organic matter maturity ranges between 0.5% and 0.85%, marked by the onset of calcite cementation and dissolution. During this phase, pore sizes and porosity decrease further, with intergranular and intercrystalline pores persisting and some dissolution pores emerging.

In the maturity range of 0.85% to 1.15%, hydrocarbon generation and dissolution by organic matter facilitate the development of additional dissolution pores, while soluble organic matter partially fills micropores. This stage witnesses enlarged pore sizes and an increased porosity, with pore types transitioning from primarily intergranular and intercrystalline to a mix dominated by intergranular and dissolution pores, along with the initial appearance of organic pores.

When Ro > 1.15, soluble organic matter undergoes cracking, and the clay mineral transformation restores previously filled micropores. Clay-mineral-related intercrystalline pores emerge, accompanied by decreased pore sizes and porosity. The pore types gradually shift to being dominated by intercrystalline pores, with a minority of organic pores.

On the whole, the dissolution of organic acid emissions in the process of organic matter hydrocarbon generation can promote porosity and pore connectivity. Although the TOC of type A3 lithofacies is relatively lower than that of A1, the higher content of rigid particles (such as quartz and feldspar) can form a support skeleton and protect the residual primary pores. The A3 type belongs to the reservoir with dominant lithofacies.

6. Conclusions

This paper conducts a detailed investigation into the pore structure characteristics and controlling factors of various lithofacies types within the first section of the Qingshankou Formation in the Daqingzijing area, Southern Songliao Basin. The key findings are summarized as follows:

1. The fine-grained sediments of the first member of the Qingshankou Formation in the Daqingzijing area of the Southern Songliao Basin are mainly composed of clay minerals, quartz and feldspar. The lithofacies types can be divided into four categories and six subcategories. They are mainly A1 (clay laminated clayey shale), A2 (clay laminated felsic shale), A3 (silty laminated felsic shale), B (blocky compacted), C (silty compacted and argillaceous shale) and D (siltstone). The A3 type is due to the high content of silty lamina. It has a high brittle mineral content, and the proportion of pore size in different lithofacies is different.
2. Sedimentation mainly controls the development of reservoir pore structure through the brittle mineral content, organic matter abundance, and degree of thermal evolution. In terms of the mineral content, the lithofacies with a high brittle mineral content have a stronger anti-compaction effect and more retained primary pores. Therefore, the pore throat structure of type A3 lithofacies with a high quartz feldspar content is better. The influence of organic matter on reservoir quality manifests in two ways. An

appropriate organic matter content produces organic acid in the process of thermal evolution to promote the formation of secondary dissolution pores in mudstone and sandstone near the mudstone section and, at the same time, provides a material basis for later organic matter pores. However, an excessive organic matter content will block the pores and reduce the compressive strength of the rock, which is not conducive to the pore preservation of the rock.

3. The A3 (silty laminated felsic shale) shale reservoir has the most favourable lithofacies in the study area and experienced a pore evolution process characterised by "two drops and two rises": compaction, cementation and pore reduction; dissolution and pore increase; and organic matter cracking and pore increase.

Author Contributions: Conceptualization, X.W., Y.S., and T.W.; methodology, B.Y.; validation, R.L. and B.Y.; formal analysis, X.W. and Y.S.; investigation, Y.S.; resources, T.W. and B.Y.; data curation, T.W.; writing—original draft preparation, X.W.; writing—review and editing, X.W. and R.L.; visualization, R.L.; supervision, Y.S. and B.Y.; funding acquisition, T.W. All authors have read and agreed to the published version of the manuscript.

Funding: This research was funded by the Project of Sanya Yazhou Bay Science and Technology City (No. SCKJ-JYRC-2022-09) and Heilongjiang Provincial Natural Science Foundation of China (No. ZD2023D002).

Data Availability Statement: All relevant data are contained within the paper.

Conflicts of Interest: The authors declare no conflicts of interest.

References

1. Zou, C.; Tao, S.; Yang, Z.; Yuan, X.; Zhu, R.; Hou, L.; Jia, J.; Wang, L.; Wu, S.; Bai, B.; et al. New Advance in Unconventional Petroleum Exploration and Research in China. *Bull. Mineral. Petrol. Geochem.* **2012**, *31*, 312–322.
2. Wei, Y.; Ran, Q.; Tong, M.; Wang, Z. A full cycle productivity prediction model of fractured horizontal well in tight oil reservoirs. *J. Southwest Pet. Univ. (Sci. Technol. Ed.)* **2016**, *38*, 99–106.
3. Zhao, W.; Jia, A.; Wei, Y.; Wang, J.; Zhu, H. Progress in shale gas exploration in China and prospects for future development. *China Pet. Explor.* **2020**, *25*, 31–44.
4. Zou, C.; Zhao, Q.; Cong, L.; Wang, H.; Shi, Z.; Wu, J.; Pan, S. Development progress, potential and prospect of shale gas in China. *Nat. Gas Ind.* **2021**, *41*, 1–14.
5. Jin, Z.; Zhu, R.; Liang, X.; Shen, Y. Several issues worthy of attention in current lacustrine shale oil exploration and development. *Pet. Explor. Dev.* **2021**, *48*, 1471–1484. [CrossRef]
6. Liu, B.; Wang, H.; Fu, X.; Bai, Y.; Bai, L.; Jia, M.; He, B. Lithofacies and depositional setting of a highly prospective lacustrine shale oil succession from the Upper Cretaceous Qingshankou Formation in the Gulong sag, northern Songliao Basin, northeast China. *AAPG Bull.* **2019**, *103*, 405–432. [CrossRef]
7. Liu, H.; Zhang, S.; Song, G.; Wang, X.; Teng, J.; Wang, M. Effect of shale diagenesis on pores and storage capacity in the paleogene Shahejie Formation, dongying depression, Bohai Bay Basin, east China. *Mar. Pet. Geol.* **2019**, *103*, 738–752. [CrossRef]
8. Zou, C.; Zhu, R.; Bai, B.; Yang, Z.; Wu, S.; Su, L.; Dong, D.; Li, X. First discovery of nano-pore throat in oil and gas reservoir in China and its scientific value. *Acta Pet. Sin.* **2011**, *27*, 1857–1864.
9. Loucks, R.; Reed, R.; Ruppel, S.; And, D.; Jarvie, D. Morphology, genesis, and distribution of nanometer-scale pores in siliceous mudstones of the mississippian Barnett shale. *J. Sediment. Res.* **2009**, *79*, 848–861. [CrossRef]
10. Kirchofer, A.; Firouzi, M.; Psarras, P.; Wilcox, J. Modeling CO_2 transport and sorption in carbon slit pores. *J. Phys. Chem. C* **2017**, *121*, 21018–21028. [CrossRef]
11. Bernard, S.; Wirth, R.; Schreiber, A.; Schulz, H.; Horsfield, B. Formation of nanoporous pyrobitumen residues during maturation of the Barnett shale (fort worth basin). *Int. J. Coal Geol.* **2012**, *103*, 3–11. [CrossRef]
12. Jie, X.; Yan, Z.; Yang, W.; Chen, S.; Jiang, Z. Structural deformation and its pore-fracture system response of the Wufeng-Longmaxi shale in the Northeast Chongqing area, using FE-SEM, gas adsorption, and SAXS. *J. Pet. Sci. Eng.* **2022**, *209*, 109877.
13. Xie, X.; Deng, H.; Fu, M.; Hu, L.; He, J. Evaluation of pore structure characteristics of four types of continental shales with the aid of low-pressure nitrogen adsorption and an improved FE-SEM technique in Ordos Basin, China. *J. Pet. Sci. Eng.* **2020**, *197*, 108018. [CrossRef]
14. Peng, S.; Zhang, T.; Loucks, R.; James, S. Application of mercury injection capillary pressure to mudrocks: Conformance and compression corrections. *Mar. Pet. Geol.* **2017**, *88*, 30–40. [CrossRef]
15. Han, H.; Guo, C.; Zhong, N.; Pang, P.; Gao, Y. A study on fractal characteristics of lacustrine shales of Qingshankou Formation in the Songliao Basin, northeast China using nitrogen adsorption and mercury injection methods. *J. Pet. Sci. Eng.* **2020**, *193*, 107378. [CrossRef]

16. Zhang, F.; Jiang, Z.; Sun, W.; Li, Y.; Zhang, X.; Zhu, L.; Wen, M. A multiscale comprehensive study on pore structure of tight sandstone reservoir realized by nuclear magnetic resonance, high pressure mercury injection and constant-rate mercury injection penetration test. *Mar. Pet. Geol.* **2019**, *109*, 208–222. [CrossRef]
17. Mastalerz, M.; He, L.; Melnichenko, Y.; Rupp, J. Porosity of coal and shale: Insights from gas adsorption and SANS/USANS techniques. *Energy Fuels* **2012**, *26*, 5109–5120. [CrossRef]
18. Clarkson, C.; Freeman, M.; He, L.; Agamalian, M.; Melnichenko, Y.; Mastalerz, M.; Bustin, R.; Radlinski, A.; Blach, T. Characterization of tight gas reservoir pore structure using USANS/SANS and gas adsorption analysis. *Fuel* **2012**, *95*, 371–385. [CrossRef]
19. Huang, Z.; Chen, J.; Wang, Y.; Deng, C.; Xue, H. Pore Distribution of Source Rocks as Reavealed by Gas Adsorption and Mercury Injection Methods: A Case Study on the First Member of the Cretaceous Qingshankou Formation in the Songliao Basin. *Geol. Rev.* **2013**, *59*, 587–594.
20. Kuang, L.; Hou, L.; Wu, S.; Cui, J.; Tian, H.; Zhang, L. Organic matter occurrence and pore-forming mechanisms in lacustrine shales in China. *Pet. Sci.* **2022**, *19*, 1460–1472. [CrossRef]
21. Curtis, M.; Ambrose, R.; Sondergeld, C.; Rai, C. Transmission and Scanning Electron Microscopy Investigation of Pore Connectivity of Gas Shales on the Nanoscale. In Proceedings of the North American Unconventional Gas Conference and Exhibition, The Woodlands, TX, USA, 14–16 June 2011; Society of Petroleum Engineers: Kuala Lumpur, Malaysia, 2011; Volume 6.
22. Milliken, K.; Rudnicki, M.; Awwiller, D.; Zhang, T. Organic matter–hosted pore system, Marcellus Formation (Devonian), Pennsylvania. *AAPG Bull.* **2013**, *97*, 177–200. [CrossRef]
23. Curtis, M.; Cardott, B.; Sondergeld, C.; Rai, C. Development of organic porosity in the Woodford Shale with increasing thermal maturity. *Int. J. Coal Geol.* **2012**, *103*, 26–31. [CrossRef]
24. He, W.; Zhu, R.; Cui, B.; Zhang, S.; Meng, Q.; Bai, B.; Feng, Z.; Lei, Z.; Wu, S.; He, K.; et al. The geoscience frontier of Gulong shale oil: Revealing the role of continental shale from oil generation to production. *Engineering* **2023**, *28*, 79–92. [CrossRef]
25. Hart, B.; Schieber, J.; Kalinec, J. Clay diagenesis and overpressure development in upper cretaceous and tertiary shales of south Texas. *Mar. Pet. Geol.* **2023**, *147*, 105978. [CrossRef]
26. Liang, C.; Cao, Y.; Liu, K.; Jiang, Z.; Wu, J.; Hao, F. Diagenetic variation at the lamina scale in lacustrine organic-rich shales: Implications for hydrocarbon migration and accumulation. *Geochim. Cosmochim. Acta* **2018**, *229*, 112–128. [CrossRef]
27. Teng, J.; Qiu, L.; Zhang, S.; Ma, C. Origin and diagenetic evolution of dolomites in Paleogene Shahejie Formation lacustrine organic shale of Jiyang Depression, Bohai Bay Basin, East China. *Pet. Explor. Dev.* **2022**, *49*, 1251–1265. [CrossRef]
28. Chen, L.; Zhang, H.; Liang, J.; Zhu, H.; Zheng, Y. Effect of burial processes on the evolution of organic acids and implications for acidic dissolution from a case study of the Nanpu Sag, Bohai Bay Basin, China. *J. Nat. Gas Sci. Eng.* **2017**, *39*, 173–187. [CrossRef]
29. Chen, Q.; Xu, X.; Wang, S.; Li, W.; He, S.; Yang, H. Dissolution pores in shale and their influence on reservoir quality in Damintun Depression, Bohai Bay Basin, East China: Insights from SEM images, N2 adsorption and fluid-rock interaction experiments. *Mar. Pet. Geol.* **2020**, *117*, 104394. [CrossRef]
30. Sun, N.; Chen, T.; Gao, J.; Zhong, J.; Huo, Z.; Qu, J. Lithofacies and reservoir characteristics of saline lacustrine fine-grained sedimentary rocks in the northern Dongpu Sag, Bohai Bay Basin: Implications for shale oil exploration. *Asian Earth Sci.* **2023**, *252*, 105686. [CrossRef]
31. Loucks, R.; Reed, R.; Ruppel, S.; Hammes, U. Spectrum of pore types and networks in mudrocks and a descriptive classification for matrix-related mudrock pores. *AAPG Bull.* **2012**, *96*, 1071–1098. [CrossRef]
32. Zhou, Y.; Ji, Y.; Zhang, S.; Wan, L. Controls on reservoir quality of Lower Cretaceous tight sandstones in the Laiyang Sag, Jiaolai Basin, eastern China: Integrated sedimentologic, diagenetic and microfracturing data. *Mar. Pet. Geol.* **2016**, *76*, 26–50. [CrossRef]
33. Xiao, D.; Zheng, L.; Xing, J.; Wang, M.; Wang, R.; Guan, X.; Guo, X. Coupling control of organic and inorganic rock components on porosity and pore structure of lacustrine shale with medium maturity: A case study of the Qingshankou Formation in the southern Songliao Basin. *Mar. Pet. Geol.* **2024**, *164*, 106844. [CrossRef]
34. Wang, X.; Wang, M.; Li, J.; Shao, H.; Deng, Z.; Wu, Y. Thermal maturity: The controlling factor of wettability, pore structure, and oil content in the lacustrine Qingshankou shale, Songliao Basin. *J. Pet. Sci. Eng.* **2022**, *215*, 110618. [CrossRef]
35. Shen, R.; Xu, R.; Li, Y. Microscopic pore structure and solid-liquid force of Chang 73 shale in Ordos basi. *J. Cent. South Univ. (Sci. Technol.)* **2024**, *55*, 2208–2221.
36. Lin, T.F.; Fu, X.L.; Ai, X. Lithofacies types and cycle patterns of shale layers of Qingshankou Formation in Gulong Sag, Songliao Basin. *World Geol.* **2024**, *43*, 378–389.
37. Zhang, H.; Feng, Y.L.; Yang, Z. Shale oil reservoir characteristics and its formation mechanism within alkline lacustrine basins: A case study of the Fengcheng Formation in Mahu sag, Junggar basin, China. *Acta Geol. Sin.* **2024**, 1–16.
38. Sun, L.; Liu, H.; He, W.; Li, G.; Zhang, S.; Zhu, R. An analysis of major scientific problems and research paths of Gulong shale oil in Daqing Oilfield, NE China. *Pet. Explor. Dev.* **2021**, *48*, 527–540. [CrossRef]
39. Liu, C.; Xu, X.; Liu, K.; Bai, J.; Liu, W.; Chen, S. Pore-scale oil distribution in shales of the Qingshankou Formation in the changling sag, Songliao Basin, NE China. *Mar. Pet. Geol.* **2020**, *120*, 104553. [CrossRef]
40. Bruce, C.H. Smectite dehydration—Its relation to structural development and hydrocarbon accumulation in northern Gulf of Mexico basin. *AAPG Bull.* **1984**, *68*, 673–683.
41. Schmitt, M.; Fernandes, C.; Cunha Neto, J.; Wolf, F.; Dos Santos, V. Characterization of pore systems in seal rocks using nitrogen gas adsorption combined with mercury injection capillary pressure techniques. *Mar. Pet. Geol.* **2013**, *39*, 138–149. [CrossRef]

42. Feng, Z.; Jia, C.; Xie, X.; Zhang, S.; Feng, Z.; Cross, T. Tectonostratigraphic units and stratigraphic sequences of the nonmarine Songliao basin. *Basin Res.* **2010**, *22*, 79–95.
43. Wang, X.; Sun, Y.; Liu, R.; Li, Z. Research progress into fine-grained sedimentary rock characteristics and formation in a continental lake basin. *Acta Sedimentol. Sin.* **2023**, *41*, 349–377.
44. Li, Z.; Chen, J.; Zou, H.; Wang, C.; Meng, Q.; Liu, H.; Wang, S. Mesozoic–Cenozoic tectonic evolution and dynamics of the Songliao Basin, NE Asia: Implications for the closure of the Paleo-Asian Ocean and Mongol-Okhotsk Ocean and subduction of the Paleo-Pacific Ocean. *Earth-Sci. Rev.* **2021**, *218*, 103471. [CrossRef]
45. Liu, R.; Sun, Y.; Wang, X.; Yan, B.; Yu, L.; Li, Z. Production Capacity Variations of Horizontal Wells in Tight Reservoirs Controlled by the Structural Characteristics of Composite Sand Bodies: Fuyu Formation in the Qian'an Area of the Songliao Basin as an Example. *Processes* **2023**, *11*, 1824. [CrossRef]
46. Wu, H.; Zhang, S.; Jiang, G.; Huang, Q. The floating astronomical time scale for the terrestrial Late Cretaceous Qingshankou Formation from the Songliao Basin of Northeast China and its stratigraphic and paleoclimate implications. *Earth Planet. Sci. Lett.* **2009**, *278*, 308–323. [CrossRef]
47. Hazra, B.; Varma, K.; Bandopadhyay, K. FTIR, XRF, XRD and SEM characteristics of Permian shales, India. *J. Nat. Gas Sci. Eng.* **2016**, *32*, 239–255. [CrossRef]
48. Gao, Y.; Wang, M.; Li, Y.; Jiang, Z.; Deng, Y.; Qin, J. Multi-scale pore structure characterization of lacustrine fine-grained mixed sedimentary rocks and its controlling factors: A case study of Lucaogou Formation in Jimusar Sag. *Energy Fuels* **2023**, *37*, 977–992. [CrossRef]
49. Ross, D.J.; Bustin, R.M. The importance of shale composition and pore structure upon gas storage potential of shale gas reservoirs. *Mar. Pet. Geol.* **2009**, *26*, 916–927. [CrossRef]
50. He, H.; Liu, P.; Xu, L.; Hao, S.; Qiu, X.; Shan, C.; Zhou, Y. Pore structure representations based on nitrogen adsorption experiments and an FHH fractal model: Case study of the block Z shales in the Ordos Basin, China. *J. Pet. Sci. Eng.* **2021**, *203*, 108661. [CrossRef]
51. Lastoskie, C.; Gubbins, K.E.; Quirke, N. Pore size distribution analysis of microporous carbons: A density functional theory approach. *J. Phys. Chem.* **1993**, *97*, 4786–4796. [CrossRef]
52. Jin, Z.; Liang, X.; Bai, Z. Exploration breakthrough and its significance of Gulong lacustrine shale oil in the Songliao Basin, Northeastern China. *Energy Geosci.* **2022**, *3*, 120–125. [CrossRef]
53. Loucks, R.; Ruppel, S. Mississippian Barnett shale: Lithofacies and depositional setting of a deep-water shale-gas succession in the Fort Worth Basin, Texas. *AAPG Bull.* **2007**, *91*, 579–601. [CrossRef]
54. Zhang, T.; Ellis, G.; Ruppel, S.; Milliken, K.; Yang, R. Effect of organic-matter type and thermal maturity on methane adsorption in shale-gas systems. *Org. Geochem.* **2012**, *47*, 120–131. [CrossRef]
55. Jiang, Z.; Guo, L.; Liang, C. Lithofacies and sedimentary characteristics of the silurian longmaxi shale in the southeastern Sichuan Basin, China. *J. Palaeogeogr.* **2013**, *2*, 238–251.